Journal of the European Ceramic Society **17** (1997) 1675–1683

PII: S0955-2219(97)00001-0
0955-2219/97/$17.00

Characterization of Ceramic Pastes by an Indentation Hardness Test

Brian J. Briscoe & Necati Özkan

Department of Chemical Engineering and Chemical Technology, Imperial College of Science, Technology, and Medicine, London, SW7 2BY, UK

(Received 18 April 1996; revised version received 28 November 1996; accepted 2 December 1996)

Abstract

Certain material deformation properties of a typical alumina based ceramic paste system, including the hardness (a plastic yield characteristic), the elastic modulus, a plasticity index (a measure of the relative elastic–plastic response), and a mean flow stress, are obtained using an indentation hardness test. In order to compute these material properties a contact compliance procedure, in conjunction with an analysis based upon an adaptation of the Box–Cox curve fitting method for the compliance curve, has been used. The data are used to provide a basis for identifying the optimum rheological response of the paste system for plastic forming operations. © 1997 Elsevier Science Limited.

1 Introduction

Pastes, which are, for the present purposes, highly concentrated solid particle dispersions in a viscous liquid medium, are processed in a variety of industrial applications, such as food processing and ceramic manufacturing. The common feature of these paste materials is the two-phase composition of comparatively rigid small (0·1–10·0 μm) particles combined with a viscous fluid continuum. These materials normally exhibit a complex elasto–plasto–viscous behaviour under the application of an applied stress. The materials generally have highly time and strain history flow characteristics and their response is inherently difficult to quantify. In some regimes of deformation rate the materials will exhibit an elastic character insofar as part of the imposed strain is recoverable upon the removal of the corresponding applied stress. Once flow is instituted they exhibit the characteristics of plastically deforming solids and viscous liquids, i.e. they have an apparent yield stress and may strain harden or soften and also exhibit a strain rate variation like that encountered with liquids. The relative proportion of the two phases, the surface area (particle size and particle size distribution) of the rigid particles, the particle–particle interactions and the rheology of the viscous liquid phase largely control the rheological properties of pastes. In ceramic manufacturing, ceramic powders are mixed with solvents, binders, and plasticizers to obtain processable green pastes. The pastes may then be shaped by plastic deformation into self-supporting green bodies using a suitable consolidation technique such as extrusion and rolling. Optimization of the rheology of these pastes, for a chosen shape forming technique, is required in order to develop a manufacturing procedure that is capable of delivering a suitable product with the required properties and cost. In practical terms this means producing a material that will undergo sufficient plastic flow or viscous flow so as to be capable of being formed in a coherent way and yet provide an appropriate product 'rigidity' in order that it may retain its formed shape during subsequent processing operations. The necessary flow characteristics are achieved by minimizing the yield stress and suppressing the elastic response. This provides extensive coherent flow and minimizes the necessary forming forces. The 'rigidity' conferred to the product is achieved by maximizing the apparent yield stress so that the formed body does not flow appreciably under the action of the imposed gravitational and subsequent handling forces. In practice, this means that both the effective yield strain and yield stress should be maximized to increase the work required to institute plastic flow, which implies that the elastic response or modulus should also be enhanced. Hence, there is a necessary compromise between the inherent elastic behaviour that is required, in part, in order to retain the imposed form, and the plastic flow that is required in order to achieve the required form. In practice such an optimization is invariably made

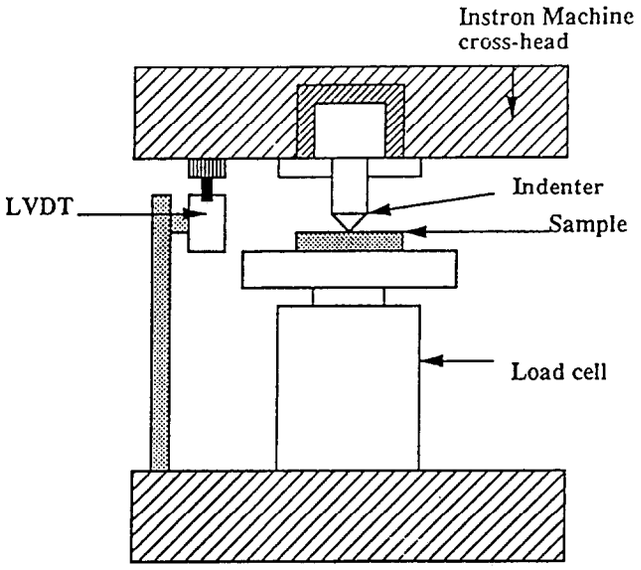

Fig. 1.Schematic view of hardness measurement apparatus.

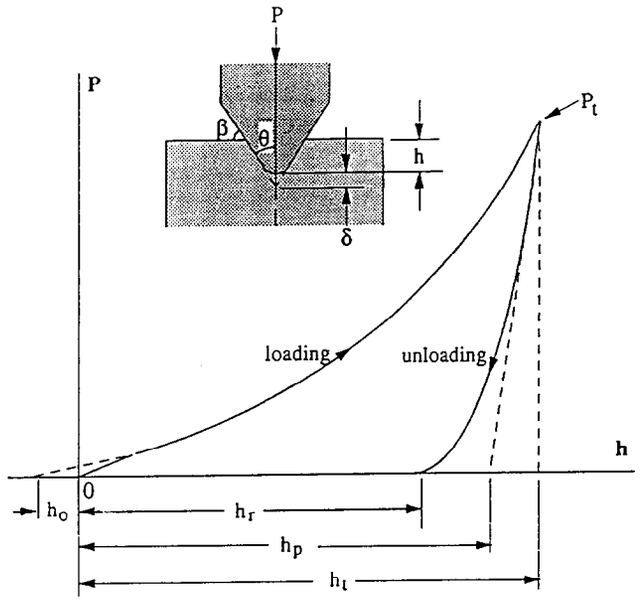

Fig. 2. Schematic diagram of contact compliance curve, P, against imposed displacement, showing the various characteristic values of the displacement, h.

on an empirical basis. For potentially complex novel formulations, a more securely founded basis for optimization is desirable. The formulation process is further complicated by the requirement to remove these processing aids during the transformation to the fully sintered state and the need to control the boundary conditions between the paste and the walls of the processing equipment.

The paper records a study of the use of an indentation hardness method as a means of characterizing the yield and the relative elastic–viscoplastic behaviours of a range of alumina based ceramic pastes. The effects of the viscous liquid medium (solvent, binder and plasticizer mixture) on the properties of the alumina pastes have been investigated. An analysis is provided to establish an index of the relative elastic to plastic response as well as the yield stress. The value of this index as a means to establish the compositions of the optimal formulations is discussed. The effects of varying the imposed strain and strain rates are also considered.

2 Indentation hardness test and introduction to data analysis

The indentation hardness test, where an indenter induces a localized deformation into a sample surface, is a relatively simple and uniquely attractive method for assessing material flow properties and in some cases the associated elastic response. A common experimental configuration, which is adopted in the present study, is shown schematically in Fig. 1 where a rigid indenter deforms a plastic paste.

Two rather different methods are commonly adopted for the measurement of indentation hardness: the imaging technique and analysis of the compliance curve. The imaging technique has some inherent limitations. For example, no information regarding the elastic response of the sample is directly available in the application of this method. In contrast, the contact compliance method records the reaction force on the indenter as a function of the imposed displacement, resulting in a set of loading and unloading curves for each indentation operation. Figure 2 illustrates the general features of typical experimental compliance curves noted in practice and introduces the various parametric notations that will be adopted. The figure also shows a schematic representation of the contact between a rigid conical indenter and a deforming substrate; the semi-induced angle of the cone is θ and angle β is the angle that the indenter makes with the planar substrate. Figure 2 also shows the case where the conical indenter contains a rounded tip whose size is characterized by a length, δ, the so-called tip defect.[1] The compliance curve will be influenced by the value of δ, and hence for small indents ($h \sim \delta$) a consideration of the magnitude of the tip defect is necessary. In the present work, experiments were performed where $h >> \delta$ and hence the gross geometry of the indenter, as described by β, is a sufficient description of the indenter geometry. For the general case of an elasto-plastic deformation, which is shown in Fig. 2, there is an appreciable elastic recovery, along the indenter loading axis, during the unloading phase. The material properties, as opposed to the contact geometry and boundary condition, which define the form of the loading curve, are the plastic yield stress and the elastic

modulus. The form of the unloading portion is largely governed by the elastic properties of the material. Thus, these compliance curves, combined with an appropriate analysis, provide the required information about both the plastic and elastic properties of the material; the time (strain rate) and strain dependence of these characteristics may also be specified to some degree.

The characteristics of the unloading curve for an elasto-plastic material reflect the elastic response of the bulk, relatively undeformed material surrounding the region of gross indentation, and also the elastic recovery within the plastically deformed indent itself. The former component dominates the initial portion of the unloading curve, which is approximately linear, whilst the latter contribution is significant towards the final part of the unloading curve. This final portion is rather non-linear in its force–displacement character. Thus, neither the depth of penetration at the maximum load, h_t, nor the residual depth of penetration, h_r provide a direct means of computing the geometry of the plastically deformed contact region (see Fig. 2). However, if the depth of penetration corresponding to the elastic recovery of the bulk material surrounding the indent is subtracted from the value h_t, what remains, the quantity h_p, may now be used to compute the geometry of the plastic indentation under load, i.e. the parameter that is obtained from the direct imaging method. The radius of the plastically deformed contact zone may then be deduced from the computed numerical value of h_p when the indenter geometry is known or assumed;[1] for conical indenters, the radius of contact, a, is equal to $h_p \tan \theta$.

The indentation hardness, H (taken here as a plastic yield characteristic), is usually defined as

$$H = \frac{P}{A} = \frac{P}{\pi a^2} \tag{1}$$

where P is the reaction force, A is the contact area projected on the original surface, and a is the corresponding radius of contact.[2] The relationship between the hardness, H, and the flow stress, σ_y, is conventionally assumed to be of the form

$$H = C\sigma_y \tag{2}$$

where C is a dimensionless constant factor whose value is a function of the material response character (the relative elastic–plastic behaviour), the contact strain, and the interface friction.[2] The value of C ranges from ca. 1·5 to 3. For a fully plastic response C is near 3 and for the cases where a significant elastic contribution is evident, C is nearer the lower limit. In the case of a fully elastic material the relationship is naturally not applicable.

The reduced elastic modulus, E^*, may be derived from the elastic contact stiffness, S, where

$$\frac{\partial P}{\partial h} = S = 2E^* a \tag{3}$$

and the reduced elastic modulus

$$E^* = \frac{E}{1 - \nu^2}$$

where E is Young's modulus and ν is Poisson's ratio. In practice, the parameter S is approximated as the elastic contact stiffness upon unloading at the maximum penetration depth, h_t (the slope of the line joining the point P_t and h_p in Fig. 2), and a is the corresponding radius of the contact zone.[3,4]

The factors that influence the computation of the values of H and E^* from the experimental compliance data have been recently reviewed by Briscoe and Sebastian.[5] Intrinsic errors arise from uncertainties in the zero point, the indenter geometry (tip defect), and the ambiguity inherent in the linear extrapolation which must be adopted in order to calculate the value of E^*, all of which influence the calculation of the hardness. The overall error may be greatly minimized by the adoption of an appropriate curve fitting procedure[6] for the experimental compliance data, from which the required various h values and slopes may be abstracted. The Box–Cox curve fitting procedure was found to be particularly attractive since it provides a physically realistic description of the contact compliance curve of the form:

$$P = m(h - h_0)^n \tag{4}$$

where h is the experimentally imposed depth of penetration, h_0 is the zero offset (see Fig. 2), m is a coefficient and n is the characteristic load index of h for the compliance curve. The Box–Cox method has been adopted in the present study. By using the Box–Cox fitting method in conjunction with the experimental data, loading and unloading curves of the following forms are obtained with the corresponding values of m and n:

$$P_1 = m_1 (h - h_0)^{n}_1 \tag{5}$$

$$P_2 = m_2 (h - h_r)^{n}_2 \tag{6}$$

where h_0 and h_r are the error and residual value of h in the loading (subscript 1) and unloading (subscript 2) curves, respectively (Fig. 2). The value of h_p is then obtained from the slope of the unloading curve at $h = h_t$, from eqn (6). A main requirement, in the current context, is to provide a measure of the relative elastic–plastic properties as well as the yield stress. The equations introduced above may be manipulated to produce a direct measure of elasto-plastic response characteristic.

The total work of indentation, W_{ep}, and its elastic and plastic components, W_e and W_p respectively, are given by[5]

$$W_{ep} = \int_0^{h_1} P_1 dh = \frac{m_1}{n_1 + 1}\{(h_1 - h_0)^{n_1+1} - (-h_0)^{n_1+1}\} \quad (7)$$

$$W_e = \int_{h_r}^{h_t} P_2 dh = \frac{m_2}{n_2 + 1}(h_t - h_r) \quad (8)$$

and

$$\phi^x = \frac{W_e}{W_p} = \frac{W_e}{W_{ep} - W_e} \quad (9)$$

The parameter ϕ^x is a plasticity index which quantifies the relative contributions of the elastic and plastic responses for the chosen deformation geometry; in the current case this is the angle β.

Alternatively, a common plasticity index which includes the geometric character of the indentation (the imposed strain) may be adopted from the precedents developed for the description of the contact mechanics of rough surfaces.[7] The inter-relationship between the hardness, H, and the reduced elastic modulus, E^*, (for perfect cones) is given as

$$\psi = \text{tab } \beta \quad \frac{E^*}{H} = \frac{\pi}{2}\left(\frac{n_2}{1 - \frac{h_r}{h_t}} - 1\right) \quad (10)$$

where β is the angle of inclination of the cone to the sample surface ($\beta = \pi/2 - \theta$). Historically, a value of ψ less than 1 indicates a primarily elastic deformation and vice versa.

The hardness indentation test may also be used to determine the creep response of a rate dependent material, either by applying a fixed load to the indenter and measuring the rate of penetration, or by pressing the indenter into the specimen at a prescribed rate and measuring the reaction load. Such a characterization is important in many facets of paste processing, not least in order to provide a measure of the product's ability to retain the imposed shape over a long period. An empirical relationship for a rate dependent material was suggested by Mulhearn and Tabor:[8]

$$\sigma = \sigma_0\left(\frac{\dot{\epsilon}}{\dot{\epsilon}_0}\right)^{1/b} \quad (11)$$

where σ_0, b and $\dot{\epsilon}_0$ are materials constants, σ ($P/\pi a^2$) is the imposed stress and $\dot{\epsilon}$ is the corresponding strain rate. Then, the stress under the indenter scales as

$$\sigma = \frac{P}{\pi a^2} = \alpha\sigma_0\left(\frac{\gamma\dot{\epsilon}^{\text{eff}}}{\dot{\epsilon}_0}\right)^{1/b} \quad (12)$$

where, α and γ are material constants which vary with b, and the 'effective strain rate', $\dot{\epsilon}^{\text{eff}}$, depends on the geometry of the indenter, the contact radius, a, and the penetration rate, $\dot{h}$. The contact strain may be approximated as 0·2 tanβ.[7] The effective strain rate imposed during normal indentation is not readily specified with any confidence. The imposed strain is, in principle, constant of the order of 0·2 tanβ and is not a function of depth for conical indenters.[2] To a first order, if the penetration rate is $\dot{h}$ and the depth of the indentation is h (the corresponding radius of contact, a, is h tanθ) then the effective strain rate is simply of the order of $\dot{h}/a$. Bower *et al.*[9] have also provided a theoretical analysis of indentation creep, and they proposed the following relationship for an axisymmetric punch:

$$\sigma = \frac{P}{\pi a^2} = \sigma_0\left(\frac{\dot{h}}{a\dot{\epsilon}_0}\right)^{1/b} F_a(b) \quad (13)$$

where $F_a(b)$ is a function that depends only upon the material parameter, b, and is independent of the shape of the indenter and $P/\pi a^2$ is defined as the mean contact pressure (mean indentation pressure). Equation (13) was adopted for the subsequent creep analysis of the pastes used in the current study.

3 Experimental procedure

3.1 Paste preparation

A commercial alumina (AES-11, Morgan Matroc, UK) with an average particle size of 0·4 μm was used to prepare a range of ceramic pastes of different rheology. A methylethylketone (MEK) (Aldrich Chemical Co., UK) –ethanol (BDH Lab. Supplies, UK) azetropic mixture was used as a solvent with a poly(vinyl butyral) (PVB) (Aldrich Chemical Co., UK) as a dispersant and a binder. Dibutyl phthalate (DBP) (Aldrich Chemical Co., UK) was used as a plasticizer. Initially, 2·0 wt% PVB was mixed with the solvent in a glass beaker, and then the alumina powders were added to the solvent mixture. In order to break down the weaker agglomerates, the suspension was ultrasonicated for 3 min using a Vibra-Cell 'Model CV26' (700 W) ultrasonicater at an amplitude of 65%. After adding the binder (PVB) and the plasticiser (DBP, the suspension was again ultrasonicated for an additional 2 min and subsequently ball-milled for 12 h in order to obtain a well-dispersed suspension. The ceramic paste was obtained by removing most of the solvent from the suspension under the action of continuous stirring in a water bath at 60°C. In order to study the effects of the solvent on the material properties of the paste, pastes with different amounts of retained solvent were prepared. The pastes with various plasticizer contents were

Table 1. Properties of ceramic pastes used in this study

Pastes	*Solvent content (wt%)*	*Binder (PVB) content (wt%)*	*Plasticizer content (wt%)*	*Plasticizer/ binder ratio*
P/75/S1	4·58	10·00	7·50	0·75
P/75/S2	3·56	10·00	7·50	0·75
P/75/S3	1·97	10·00	7·50	0·75
P/75/NS	0·00	10·00	7·50	0·75
P/100/S1	3·78	10·00	10·00	1·00
P/100/S2	2·99	10·00	10·00	1·00
P/100/S3	2·05	10·00	10·00	1·00
P/100/S4	1·31	10·00	10·00	1·00
P/100NS	0·00	10·00	10·00	1·00
P/125/S1	3·32	10·00	12·50	1·25
P/125/S2	3·07	10 00	12·5	1·25
P/125/S3	2·43	10·00	12·5	1·25
P/125/S4	1·77	10·00	12·5	1·25
P/125NS	0·00	10·00	12·5	1·25

also prepared in order to study the effects of the plasticizer content on the material properties of the ceramic paste. Table 1 summarizes the composition of the ceramic pastes studied. The binder–plasticizer mixtures, without the incorporation of the ceramic particles, were also prepared in order to elucidate the intrinsic role of the binder and plasticizer on the deformation behaviour of these ceramic pastes.

3.2 Hardness measurements

A standard universal testing machine (Instron 1122, UK) was adapted for the hardness measurement experiments, taking advantage of the load sensors and actuator available in the machine. A separate LVDT was used in order to record the imposed displacement (Fig. 1). The indenter, a steel cone (90° with a tip defect of 2 μm) was fixed in a special holder fitted to the crosshead of the testing machine; the representative strain was thus ca. 0·2. The specimen was supported on an alignment platform attached to the load cell. The typical maximum depths of penetration, h_t, were around 3 mm. In the experiments, where the indenter was driven into the pastes at a constant velocity, a range of velocities from $8{\cdot}3 \times 10^{-6}$ to $3{\cdot}3 \times 10^{-4}$ m/s were used.

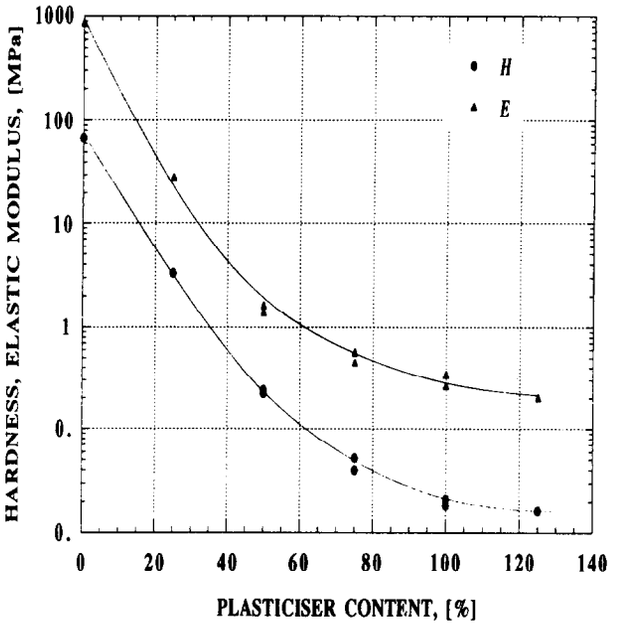

Fig. 3. Hardness and elastic modulus of binder–plasticizer mixture as a function of plasticizer content.

3.3 Glass transition temperature (T_g) measurements

The glass transition temperatures, T_g, of the binder–plasticizer mixtures with various plasticizer contents were determined using a differential scanning calorimeter DSC (Perkin Elmer). A scan speed of 20°C/min was used between –90°C and 100°C.

4 Experimental results

The material properties (the hardness, the elastic modulus, the plasticity indexes, and the mean contact pressure as a function of the effective strain rate) of the binder–plasticizer mixtures were abstracted from data obtained in the hardness indentation test using the procedures outlined in Sections 2 and 3. The results for these mixtures are summarized in Table 2. The computed hardness and elastic modulus of the binder–plasticizer mixture, as a function of the plasticizer content, are shown in Fig. 3. As may be seen from Fig. 3, both the hardness and the elastic modulus of the mixture decrease with increasing plasticizer content. The glass transition

Table 2. Parameters and calculated values of H, E^* and plasticity index for binder–plasticizer mixture containing various amounts of plasticizer. Indentation speed = 5 mm/min, S and F denote independent properties

Plasticizer content (%)	n_1	m_1	h_0 *(m)*	n_2	m_2	h_r *(m)*	H *(MPa)*	E* *(MPa)*	*Index* W_e/W_p	*Index* ψ
50 (S)	1·93	653·28	$-8{\cdot}40 \times 10^{-5}$	3·02	956·98	$9{\cdot}60 \times 10^{-4}$	0·22	1·40	0·72	6·38
75 (S)	1·63	315·76	$-8{\cdot}66 \times 10^{-5}$	2·71	860·70	$1{\cdot}42 \times 10^{-3}$	0·052	0·45	0·40	8·67
100 (S)	1·45	157·92	$-6{\cdot}20 \times 10^{-5}$	2·86	972·98	$1{\cdot}61 \times 10^{-3}$	0·018	0·26	0·21	14·70
125 (S)	1·42	138·93	$-1{\cdot}46 \times 10^{-5}$	2·60	822·22	$1{\cdot}52 \times 10^{-3}$	0·016	0·20	0·22	12·57
0 (F)	1·65	22373·3	$-1{\cdot}84 \times 10^{-5}$	2·67	22784·2	$7{\cdot}24 \times 10^{-4}$	68·72	858·31	0·27	12·49
25 (F)	1·87	2804·6	$-1{\cdot}12 \times 10^{-4}$	3·17	3290·2	$7{\cdot}78 \times 10^{-4}$	3·31	28·52	0·46	8·62
50 (F)	1·89	683·3	$-1{\cdot}32 \times 10^{-4}$	2·56	1341·6	$1{\cdot}23 \times 10^{-3}$	0·24	1·64	0·57	6·97
75 (F)	1·50	271·14	$-1{\cdot}4 \times 10^{-4}$	2·78	1254·8	$1{\cdot}68 \times 10^{-3}$	0·040	0·565	0·21	14·25
100 (F)	1·29	146·72	$-6{\cdot}62 \times 10^{-5}$	1·76	1333·9	$1{\cdot}59 \times 10^{-3}$	0·021	0·340	0·15	15·87

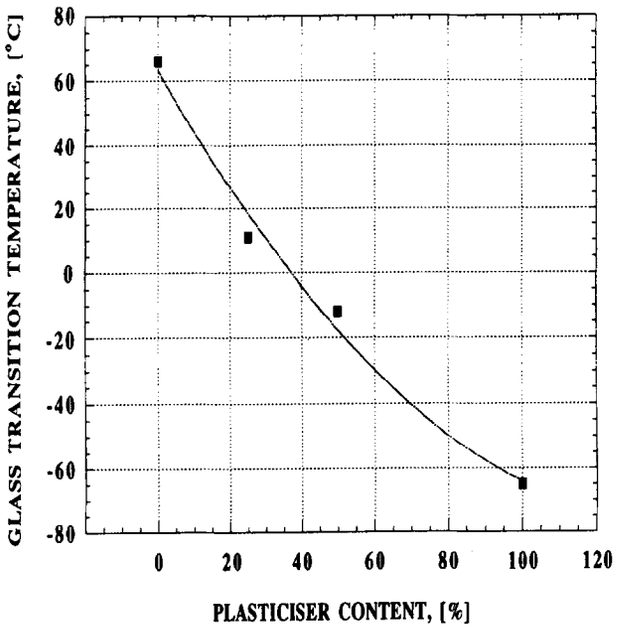

Fig. 4. Glass transition temperature of binder–plasticizer mixture as a function of plasticizer content.

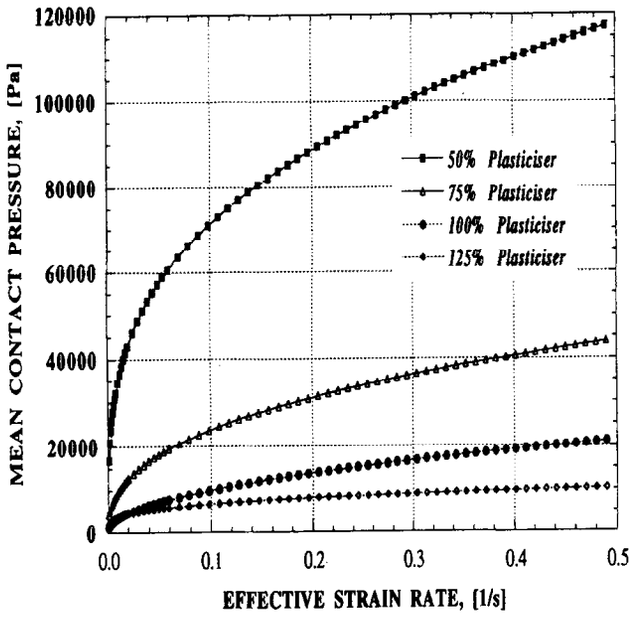

Fig. 5. Plots of mean contact pressure against effective strain rate for binder–plasticizer mixtures.

of the binder (PVB) is ca. 66°C. The glass transition temperature of the binder–plasticizer mixture, as a function of the plasticizer content, is shown in Fig. 4. As the plasticizer is added to the binder, the glass transition temperature of the system is reduced. As a result, the hardness and elastic modulus values of the mixture are decreased with the addition of the plasticizer. The mean contact pressure of the binder–plasticizer mixture, as a function of the effective strain rate, is shown in Fig. 5. The mean contact pressure of the mixture decreases with increasing plasticizer content.

The abstracted hardness indentation data for the various alumina paste systems are summarized in Tables 3 and 4. The parameters listed are the indices of the loading and unloading curves n_1, n_2, m_1 and m_2 (eqns (5) and (6)), the error parameters h_0 and h_r (eqns (5) and (6)), the computed hardness, H (eqn (1)), and the reduced elastic modulus, E^* (eqn (3)). Two plasticity indices W_e/W_p and ψ (eqns (9) and (10)) are also listed. It is clear that the material properties of the pastes are strongly influenced by the solvent content of the paste. The hardness of the alumina pastes, as a function of the solvent content, is shown in Fig. (6). The hardness and elastic modulus of the pastes are substantially increased with decreasing solvent content. The plasticizer content of the paste also has a strong influence on the properties of the paste as well as that of the continuous phase. The hardness values (and also the elastic modulus) of these two systems show similar trends, both decreasing with an increase in the plasticizer ratio (Fig. 7). The hardness values of the pastes are much higher than that of the simple binder–plasticizer mixture, and the difference becomes more pronounced as the plasticizer content decreases (Fig. 8).

The two computed plasticity indexes for the alumina pastes, with no significant solvent content, as a function of the plasticizer content are shown in Fig. 9. The index, ψ, increases with decrease in the plasticizer content and the index, ϕ^x, decreases with decrease in the plasticizer content. These results indicate that the plastic character of the paste, a viscoelasto–plastic material, increases with decreasing plasticizer content.

The mean contact pressure of a paste (10 wt% binder–10 wt% plasticizer), as a function of the effective strain rate ($\dot{h}/a$), for various solvent contents is shown in Fig. 10. The mean contact pressure of the paste is substantially reduced with the

Table 3. Parameters and calculated values of H, E^* and plasticity indexes for paste (without solvent) with different indentation speeds. The paste contains 10 wt% binder (PVB) and 10 wt% plasticizer (DBP)

Indentation speed (mm/min)	n_1	m_1	h_0 *(m)*	n_2	m_2	h_r *(m)*	H *(MPa)*	E* *(MPa)*	*Index* W_e/W_p	*Index* ψ
2	2·07	2748·80	$-2·09 \times 10^{-4}$	11·29	511·11	$1·46 \times 10^{-3}$	4·10	68·75	0·20	16·77
5	2·07	3060·68	$-1·2 \times 10^{-4}$	7·41	1076·06	$1·22 \times 10^{-3}$	4·52	82·50	0·26	18·25
10	2·07	3246·09	$-1·05 \times 10^{-4}$	8·33	942·58	$9·76 \times 10^{-4}$	5·03	92·51	0·26	18·38
20	2·20	2911·67	$-1·92 \times 10^{-4}$	10·0	657·50	$6·87 \times 10^{-4}$	5·62	103·51	0·27	18·42

Table 4. Parameters and calculated values of H, E* and plasticity indexes for pastes with different solvent contents. Indentation speed = 5 mm/min

Pastes %B–%P	*Solvent content (%)*	n_1	m_1	h_0	n_2	m_2	h_r *(m)*	H *(MPa)*	E* *(MPa)*	*Index* W_e/W_p	*Index* ψ
10·0–7·5	4·58	1·41	246·68	$-1{\cdot}64 \times 10^{-4}$	2·97	1226·08	$2{\cdot}79 \times 10^{-3}$	0·026	0·51	0·15	19·66
10·0–7·5	3·56	1·55	673·49	$-8{\cdot}26 \times 10^{-5}$	3·13	1924·18	$2{\cdot}87 \times 10^{-3}$	0·115	2·35	0·16	20·38
10·0–7·5	1·97	1·52	2909·01	$-3{\cdot}05 \times 10^{-5}$	4·48	3793·7	$1{\cdot}83 \times 10^{-3}$	1·20	37·06	0·11	30·91
10·0–7·5	0·00	1·70	14672·17	$-3{\cdot}79 \times 10^{-5}$	3·89	11165·8	$1\ 68 \times 10^{-3}$	27·86	838·8	0·12	30·11
10·0–10·0	3·78	1·30	215·72	$-3{\cdot}05 \times 10^{-5}$	3·44	854·62	$1{\cdot}40 \times 10^{-3}$	0·031	0·38	0·25	12·20
10·0–10·0	2·99	1·46	389·51	$-7{\cdot}05 \times 10^{-5}$	3·19	1261·22	$1{\cdot}70 \times 10^{-3}$	0·062	1·01	0·22	14·44
10·0–10·0	2·05	1·60	622·96	$-5{\cdot}15 \times 10^{-5}$	3·26	1794·37	$1{\cdot}77 \times 10^{-3}$	0·129	2·05	0·25	15·90
10·0–10·0	1·31	1·64	1099·97	$-4{\cdot}66 \times 10^{-5}$	3·23	2099·28	$1{\cdot}38 \times 10^{-3}$	0·365	4·73	0·27	12·97
10·0–10·0	0·00	2·07	3060·68	$-1{\cdot}2 \times 10^{-4}$	7·41	1076·06	$1{\cdot}22 \times 10^{-3}$	4·52	82·50	0·26	18·25
10·0–12·5	3·32	1·39	143·51	$-1{\cdot}80 \times 10^{-4}$	2·82	459·48	$1{\cdot}80 \times 10^{-3}$	0·014	0·12	0·37	8·21
10·0–12·5	3·07	1·52	178·21	$-1{\cdot}52 \times 10^{-4}$	3·69	553·32	$2{\cdot}17 \times 10^{-3}$	0·017	0·20	0·27	12·34
10·0–12·5	2·43	1·50	230·25	$-9{\cdot}11 \times 10^{-5}$	2·41	904·75	$2{\cdot}35 \times 10^{-3}$	0·026	0·30	0·26	11·61
10·0–12·5	1·77	1·62	364·77	$-9{\cdot}89 \times 10^{-5}$	2·73	1311·78	$2{\cdot}35 \times 10^{-3}$	0·051	0·74	0·22	14·54
10·0–12·5	0·00	2·00	1266·49	$-1{\cdot}00 \times 10^{-4}$	4·02	1067·46	$1{\cdot}35 \times 10^{-4}$	0·739	6·78	0·52	9·17

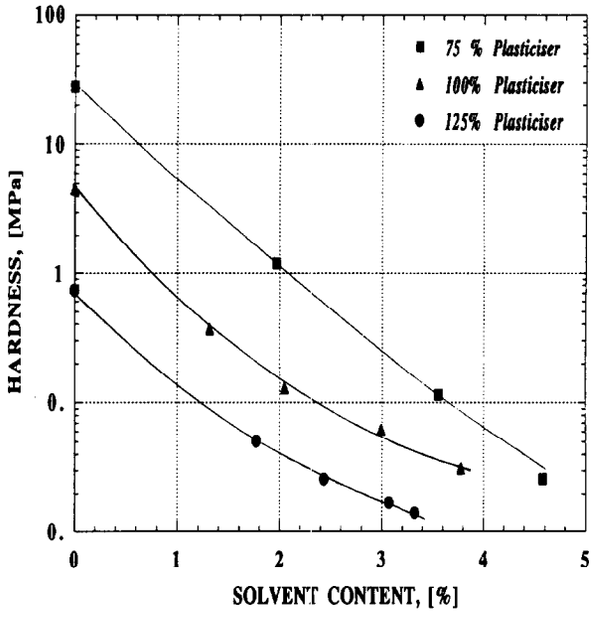

Fig. 6. Hardness of alumina pastes as a function of solvent content.

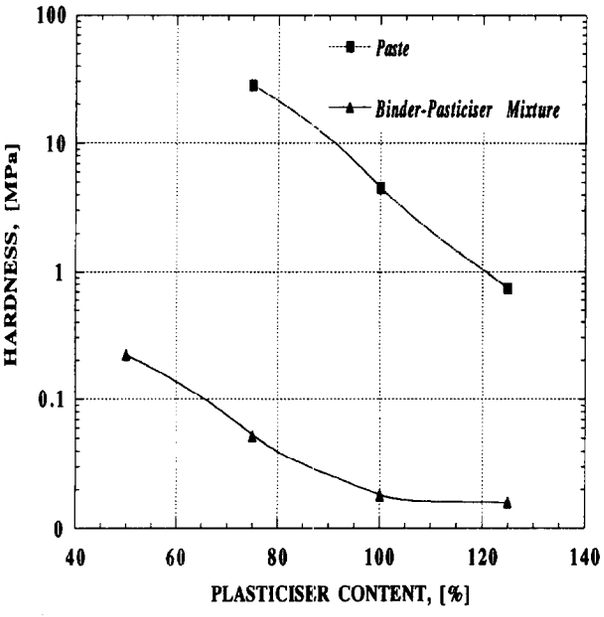

Fig. 7. Hardness of binder–plasticizer mixtures and alumina pastes with no solvent as a function of plasticizer content.

increasing solvent content. The plasticizer content also affects the mean contact pressure of the paste, the mean contact pressure of the paste is reduced with increasing plasticizer content (Fig. 11).

Thus, the compliance method provides flow characteristics that are of value in optimizing the rheology of pastes and their greens. The hardness and elastic modulus values are readily obtained. These two parameters provide a measure of the relative elastic–plastic response. For the present paste system an optimal processing rheology and the subsequent green mechanical stability was obtained at values of ψ and ϕ^x of ca. 20 and 0·25, respectively, for the case of tape forming using a two-roll mill.[10] In this forming operation the ceramic pastes were reduced in thickness by 30% using roll speeds ranging from 10 to 40 r.p.m. The mean, or effective, strain rate in the rolling process is given as[11]

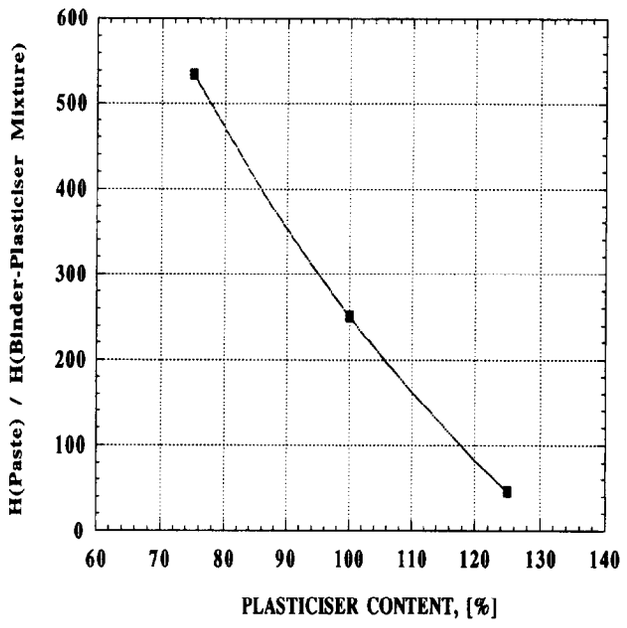

Fig. 8. Ratio of hardness value of paste to that of the binder–plasticizer mixture as a function of plasticizer content.

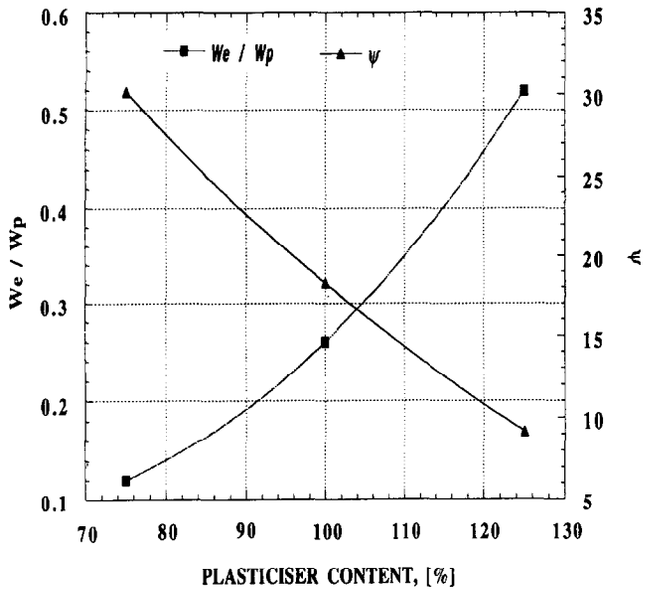

Fig. 9. Plasticity indexes as for alumina pastes as a function of plasticizer content.

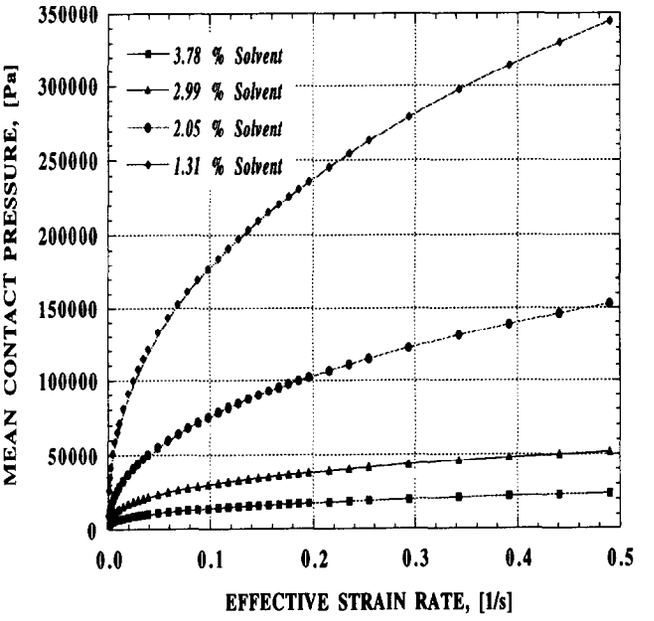

Fig. 10. Mean contact pressure against effective strain rate for alumina pastes with various solvent contents.

$$\bar{\dot{\epsilon}} \cong \omega \left(1 - \frac{3}{4} r\right) \sqrt{\frac{r}{1 - r} \frac{R}{h_2}} \tag{14}$$

where ω is the angular velocity of the rolls, r is the fractional reduction, R is the radius of the rolls and h_2 is the final thickness of the rolled tape. Equation (14) indicates that the effective strain in the rolling process depends upon the final thickness of the rolled tape. The final thickness of the rolled tapes, h_2, was between 10·0 and 0·3 mm. For a roll speed of 10 r.p.m., the effective strain rates were ca. 1 and 70 s^{-1} for final tape thicknesses of 10 and 0·3 mm, respectively.

5 Conclusions

The compliance hardness indentation test with an associated analysis has been used to characterize the rheology of a range of ceramic pastes. The viscous liquid phase of the paste, consisting of the solvent, the binder and the plasticizer, has a strong effect on the properties of the alumina paste used in this study. The hardness, the elastic modulus, and the mean contact pressure values of the pastes decrease substantially with increasing solvent content. The plasticizer content of the paste also affects the properties of the paste. The hardness, the elastic modulus, and the mean contact pressure values of the paste also decrease with increasing plasticizer content. The plasticity index, ψ, of the paste increases with decreasing plasticizer content, indicating that the paste becomes more plastic in character as the plasticizer content of the paste is reduced. In the present study the optimal paste elastic–plastic response for effective processing was identified as being in the range of $\psi = 20$ and $\phi^x = 0{\cdot}25$. Thus we conclude that the parameters ψ and ϕ^x are useful criteria for the optimization of paste rheology for subsequent processing

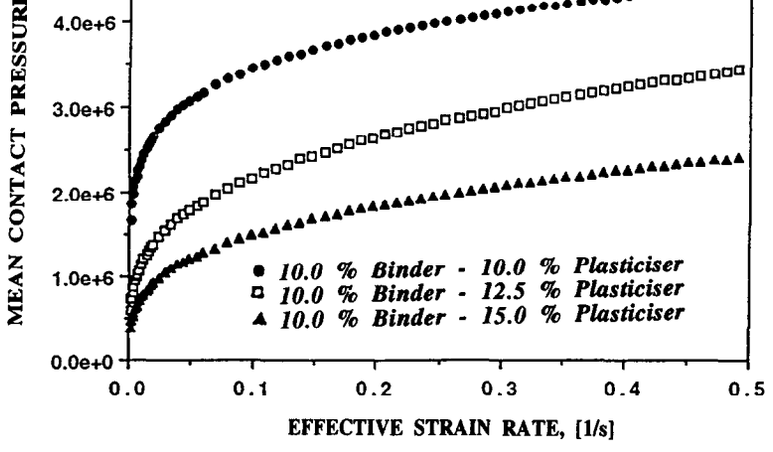

Fig. 11. Mean contact pressure against effective strain rate for alumina pastes with various plasticizer contents.

operations. In addition, the indentation method provides a direct estimation of the mean flow stress which can, in principle, be estimated as a function of the imposed strain and strain rate. These values are in the upper range of the simulations obtained for the hardness study. However, the post forming stability will be governed by a much lower ratio of deformation which will fall in the range of the strain rates generated in the hardness studies.

Acknowledgement

The authors would like to acknowledge EPSRC for their financial support.

References

1. Loubet, J. L., Georges, J. M., Meachesini, O. and Meille, G., Vickers Indentation curves of MgO. *Trans. ASME, J. Tribol.*, 1984, **106**, 43–48.
2. Tabor, D., *Hardness of Metals*. Oxford University Press, Oxford, UK, 1951.
3. Kendall, K. and Tabor, D., An ultrasonic study of the area of contact between stationary and sliding surfaces. *Proc. R. Soc. Lond.*, 1971, **A323**, 321–340.
4. Pharr, G. M., Oliver, W. C. and Brotzen, F. R., On the generality of the relationship among contact stiffness, contact area, and elastic modulus during indentation. *J. Mater. Res.*, 1992, **7**, 613–617.
5. Briscoe, B. J. and Sebastian, S., The elastic response of poly (methyl methacrylate) to indentation. *Proc. R. Soc. Lond.*, 1996, **A452**, 439–457.
6. Box, G. E. P. and Cox, D. R., An analysis of transformations. *J. R. Statistical Soc.*, 1964, **26**, 211–243.
7. Johnson, K. L., *Contact Mechanics*. Cambridge Press, Cambridge, 1985.
8. Mulhearn, T. O. and Tabor, D., Creep and hardness of metals: a physical study. *J. Inst. Met.*, 1960, **89**, 7.
9. Bower, A. F., Fleck, N. A., Needleman, A. and Ogbonna, N., Indentation of a power law creeping solid. *Proc. R. Soc. Lond.*, 1993, **A441**, 97–124.
10. Özkan, N. and Briscoe, B. J., Preparation of ceria–gadolinia electrolytes by tape rolling technique, *J. Mater Res.*, in press.
11. Chakrabarty, J., *Theory of Plasticity*. McGraw Hill Book Company, New York, 1987, p.581.